

Optoelectronic and photocatalytic properties of in situ platinum-doped TiO₂ films deposited by means of pulsed laser ablation technique

K. Trabelsi^{1,2,4} · A. Hajjaji^{1,2} · I. Ka¹ · M. Gaidi³ · B. Bessais² · M. A. El Khakani¹

Received: 26 August 2016 / Accepted: 20 October 2016 / Published online: 26 October 2016
© Springer Science+Business Media New York 2016

Abstract We report on the effect of Pt incorporation on the microstructural, optoelectronic and catalytic properties of TiO₂ thin films deposited by means of the pulsed-laser deposition (PLD) method. The structural, morphological, optoelectronic and catalytic properties of the deposited TiO₂:Pt films were systematically investigated, as a function of their Pt content, by means of various techniques including X-ray diffraction, X-ray photoelectron spectroscopy (XPS), atomic force microscopy, Fourier-transform infra-red spectroscopy and ellipsometry. The in situ doping of the PLD-TiO₂ films, at different Pt contents, was achieved by the concomitant laser ablation of a TiO₂ target uniformly covered with Pt wires. We show that by increasing the number of Pt wires positioned on the TiO₂ target from 1 to 4, the Pt concentration of the TiO₂:Pt films increases from 0.05 to 0.35 at.%. While the bandgap of room-temperature (RT) deposited films was found to be insensitive to their Pt content (remaining around the 3.2 eV anatase value), the TiO₂:Pt films deposited at high temperature ($T_d = 500$ °C) were found to exhibit a significant

narrowing of their bandgap (from 3.3 to 2.45 eV), when their Pt content is increased (from 3.3 to 2.45 eV). From a structural point of view, while the RT-deposited TiO₂:Pt films deposited are mainly amorphous with the presence of some TiO₂ nanocrystallites whose density increases as Pt content increases, while those deposited at 500 °C were found to crystallize in the anatase phase with their crystallinity improving with increasing Pt contents. XPS analyses have revealed that the incorporated Pt mainly exists in a metallic state, likely as nano-inclusions in an otherwise TiO₂ matrix. By being able to monitor the optoelectronic properties of the annealed TiO₂:Pt films through their Pt content, their photocatalytic activity was significantly improved with respect to that of their undoped TiO₂ counterpart. The enhancement of the photocatalytic activity is believed to be due to an enhanced photoabsorption of photons because of bandgap narrowing along with a better harvesting of the separated photogenerated charges.

1 Introduction

During the last decade, there has been extensive research activity on photocatalysis using the well-known titanium dioxide (TiO₂), which is a large bandgap semiconductor with many interesting photoactive properties [1, 2] and electrochemical stability [3]. Recently novel efficient photoactive nanocomposites like ZnWO₄ and CdMoO₄ have been prepared using simple and low cost methods such as the precipitation and sol gel methods [4, 5]. However, TiO₂ remains, and by far, the most widely used photocatalyst because of not only its abundance and relatively low cost, but also for its unpaired optoelectronic properties, such as its high refractive index. This combination of unique properties has widened the application of

✉ M. Gaidi
mkaidi@sharjah.ac.ae

¹ Institut National de la Recherche Scientifique, INRS-Énergie, Matériaux et Télécommunications, 1650, Blvd. Lionel-Boulet, Varennes, QC J3X-1S2, Canada

² Laboratoire de Photovoltaïque, Centre de Recherches et des Technologies de l'Énergie, Technopole de Borj-Cédria, BP 95, 2050 Hammam-Lif, Tunisia

³ Center for Advanced Materials Research, University of Sharjah, PO Box 27272, Sharjah, United Arab Emirates

⁴ Université de tunis El Manar, BP 94, Rommana, 1068 Tunis, Tunisia

TiO₂ to many fields, such as optical devices [6], energy conversion [7], gas sensing [8], photocatalysis [1] and hydrogen production [9]. Despite all these properties, the relatively large band gap of TiO₂ (3.2 eV for the anatase phase) limits its absorption to the UV range and thereby only a small portion (~5 %) of the solar spectrum can be potentially used for photoconversion [10]. Thus, there is a clear need for narrowing the bandgap of TiO₂ to make more sensitive to the visible light. Such an approach based on the in situ nitrogen doping of sputtered TiO₂ films has been recently shown to be quite effective in significantly red-shifting the bandgap to the maximum solar irradiance [11].

Another challenge in photocatalytic materials is to ensure an efficient harvesting of the photo-generated charges and minimize their subsequent recombination. Therefore, developing high quantum efficiency photocatalysts which are sensitive to visible light is one of the most important topics in the photocatalysis research field. For this reason, considerable efforts have been undertaken to narrow the band gap of the photocatalyst and to reduce the recombination rate of photogenerated pair. Metal doping is one of the avenues that has been largely explored. In fact, incorporation of metallic elements in TiO₂ modifies the size and morphology of the TiO₂ nanoparticles, leading to a phase change within the crystal structure, which in turn alter the band gap of the photocatalyst. Many deposition methods have been used to prepare Pt-doped TiO₂, including sol–gel [12, 13], electrophoresis deposition [14] and pulsed laser deposition (PLD) [15]. The PLD is a highly energetic process that enables the deposition of highly pure films with good mechanical adherence [16] and relatively large specific surface area [17] suitable for sensors and photocatalytic applications. In addition, the PLD offers a large process latitude and flexibility to control of the film properties by quasi-independently adjusting the different experimental parameters (such as, target composition, nature of background gas, ambient pressure, substrate temperature, laser intensity, etc.).

In this paper, we report on the structural, morphological, optoelectronic and photocatalytic properties of in situ Pt-doped TiO₂ deposited by means of a PLD process. The chemical composition of TiO₂:Pt films and the oxidation state of platinum were studied by means of XPS. The structural, morphological and optical behaviors of the TiO₂:Pt films have been investigated using XRD, SEM, AFM, and ellipsometry. The effect of Pt content and deposition temperature on the photocatalytic activity of the PLD-TiO₂:Pt films was investigated.

2 Experimental

A KrF excimer laser (wavelength = 248 nm, pulse duration 12 ns) operating at a repetition rate of 30 Hz was focused, at an incidence angle of 45°, onto a TiO₂ rotating target (99.9 % purity). The on-target laser energy density was set to 6 J/cm². The TiO₂ thin films were deposited on two types of conventionally cleaned Si and quartz substrates. The substrates were mounted on a substrate holder and placed parallel to the target at a perpendicular distance of 6.5 cm. During the deposition step, the substrate holder may be heated while rotating, ensuring thus the uniformity of the film thickness. The TiO₂ deposition was carried out at room temperature (RT) and at a deposition temperature (T_d) of 500 °C under a background oxygen pressure of 10 mTorr. Before filling the chamber with O₂, it was first turbo-pumped to a base pressure of ~10⁻⁵ Torr. Prior to deposition, the TiO₂ target was systematically cleaned by laser-ablating its surface for 10 min while the substrate was shielded from the ablation plume by a shutter. The in situ Pt doping was achieved through the concomitant ablation of both TiO₂ target and Pt wires (0.1 cm × 5 cm) placed on the TiO₂ target surface. By exposing the target surface to the laser beam, the latter simultaneously ablates both TiO₂ and Pt wires, leading to the in situ incorporation of Pt into the growing TiO₂ films. The Pt concentration in these PLD synthesized TiO₂:Pt films can be controlled by varying the number of Pt wires (from 1 to 4), uniformly fixed on the TiO₂ target. The thickness of the TiO₂:Pt films (as estimated from SEM images) varies in the range of 400–250 nm as the Pt content increases from 0 to 0.25 at.%.

Both surface chemical composition and chemical bonding states of the TiO₂:Pt films were determined from X-ray photoelectron spectroscopy (XPS) using the ESCA-LAB 220I-XL spectrophotometer, equipped with AL-K α (1486.5 eV) monochromatic source. The morphology of the PLD deposited TiO₂:Pt films was examined via Scanning Electron Microscopy (SEM) and atomic force microscopy (AFM). The crystalline structure of the TiO₂:Pt films was investigated by means a Philips X'pert-X-ray diffractometer (Cu-k α radiation). Their optical properties have been investigated by means of ellipsometry as function of deposition temperature and doping Pt content. The TiO₂:Pt films deposited at T_d = 500 °C were used as a photocatalyst for the degradation of methyl blue under 30 min of UV radiation (256 nm, OSRAM germicidal lamp) exposure. After 30 min of photocatalysis, the concentration of the remaining colorant was measured using a UV–Vis spectrometer.

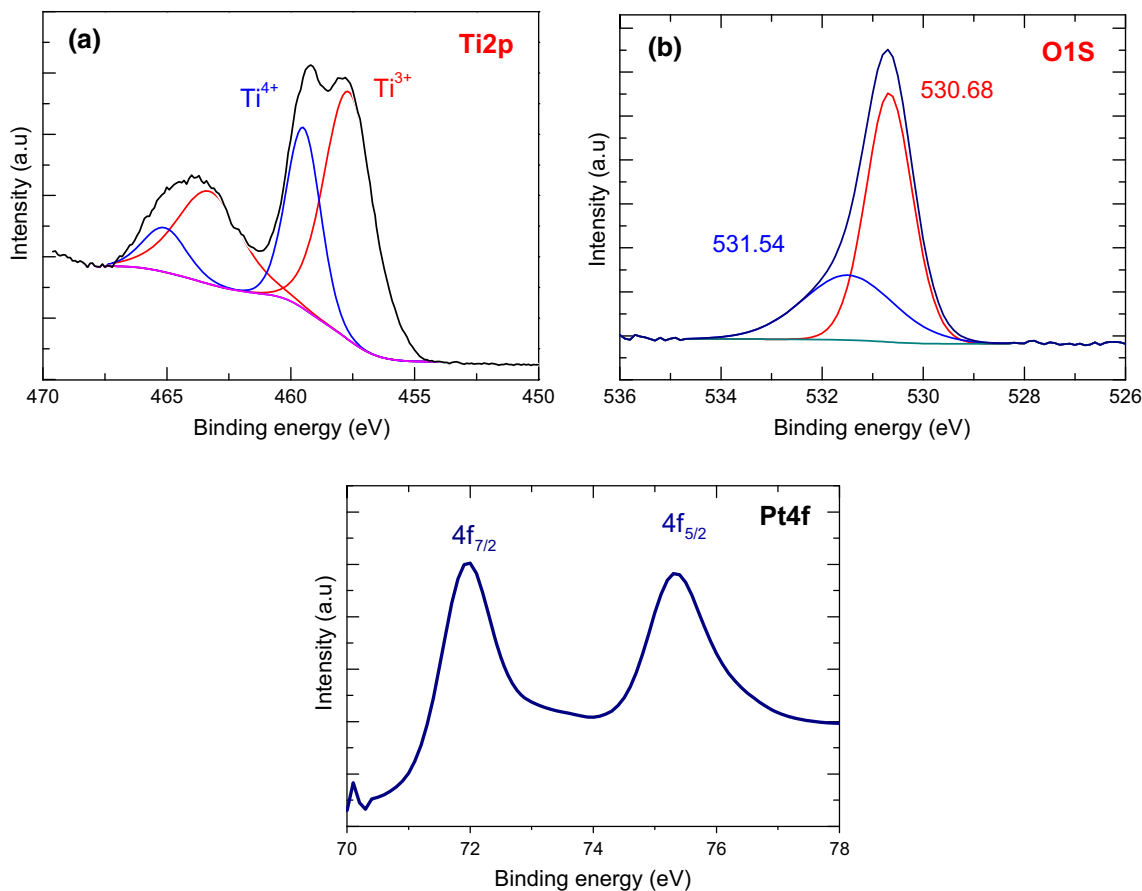


Fig. 1 Typical high-resolution XPS spectra of Ti_{2p} , O_{1s} and Pt_{4f} peaks of Pt doped TiO_2 films (3 wires of Pt) deposited at 25 °C

3 Results and discussion

The chemical composition and bonding states of the TiO_2 :Pt films were investigated by means of XPS. Figure 1 shows typical high-resolution XPS spectra of Ti_{2p} , O_{1s} , Pt_{4f} peaks of TiO_2 :Pt films (deposited with 3 Pt wires) pulsed laser deposited at 25 °C (RT). The XPS peaks related to $Ti_{2p_{3/2}}$ and $Ti_{2p_{1/2}}$ appear at 464.99 and 459.39 eV, respectively (Fig. 1a), and are assigned to Ti^{4+} [18], while the doublet localized at 463.19 and 457.55 eV is assigned to Ti^{3+} [19]. The XPS spectrum of O_{1s} (Fig. 1b) exhibits typical peaks located at 530.68 and 531.54 eV, which are ascribed to lattice oxygen in Ti–O–Ti and oxygen in surface OH^- groups, respectively [20]. The $Pt_{4f_{5/2}}$ and $Pt_{4f_{7/2}}$ peaks (Fig. 1c) are observed at 75.27 and 71.91 eV and are assigned to Pt^0 states [21].

From the XPS spectra, and by using appropriate sensitivity factors, we have calculated the Pt content of the TiO_2 :Pt films. Figure 2 shows that the Pt content of the TiO_2 :Pt films increases as the number of Pt wires positioned on the target increases in a similar way for both deposition temperatures (RT and 500 °C), and reaches its maximum for the 3 Pt wires target condition. However, it is

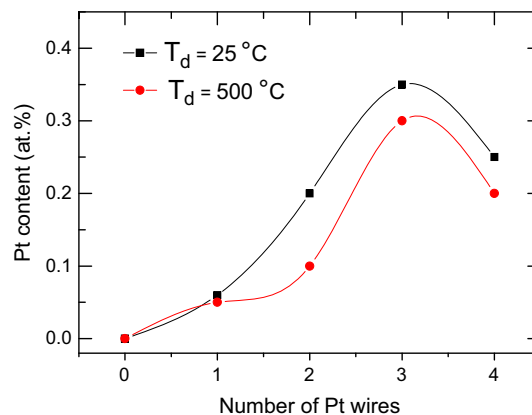


Fig. 2 Platinum content of the PLD deposited TiO_2 :Pt films as a function of the number of Pt wires

worth noting that the incorporated Pt content is slightly lower at $T_d = 500$ °C than at $T_d = 25$ °C, for the same number of Pt wires. This slightly lower Pt concentration at $T_d = 500$ °C is thought to be due to a partial evaporation of a small portion of the ablated species from the heated substrate. The maximum of Pt content is seen to reach

0.35 at.% at $T_d = 25\text{ }^\circ\text{C}$ and 0.3 at.% at $T_d = 500\text{ }^\circ\text{C}$, at the 3 Pt-wires deposition condition.

Figure 3 shows the XRD patterns of the PLD deposited $\text{TiO}_2\text{:Pt}$ films. All the films deposited at $T_d = 25\text{ }^\circ\text{C}$ are amorphous (Fig. 3a) regardless of their Pt content. However, the $\text{TiO}_2\text{:Pt}$ films deposited at $T_d = 500\text{ }^\circ\text{C}$ present a crystalline structure composed mainly of anatase phase and a weak rutile component (Fig. 3b). It is interesting to note that the ratio of anatase to rutile phases depends on the Pt content of the $\text{TiO}_2\text{:Pt}$ films. Indeed, one may notice (Fig. 3b) that the main XRD rutile peak R(110) almost disappeared beyond Pt content higher than 0.2 at.%. In fact, an inhibition of the anatase to rutile transition and grain growth may occur as the Pt doping level is increased [22, 23].

From these XRD spectra, the TiO_2 crystallite size (D) was estimated by using the Debye–Scherer method [24]. The (D) value, in a specific orientation is given by: $D = \frac{0.9\lambda}{\Delta(2\theta)\cos(\theta)}\Delta$, where (λ) is the X-ray wavelength and $\Delta(2\theta)$ the corresponding width at half maximum. The lattice constant is determined from the Bragg law and the weight fraction of the anatase phase from the Spurs formula [25]:

$$\left(W_A = \frac{I_A}{I_A + 1.265I_R}\right)$$

where I_A and I_R are the peaks intensity of anatase (101) and rutile (110) orientations, respectively, determined from the XRD patterns. All the calculated crystallite size, lattice parameter, and the anatase proportion values are gathered in Table 1. For the PLD- $\text{TiO}_2\text{:Pt}$ films deposited at $T_d = 500\text{ }^\circ\text{C}$, the anatase crystallite size was found to increase with the increase of their Pt content. The addition of Pt is also found to lead to a variation of the anatase-to-rutile ratio. Beyond 0.2 at.% of Pt, the intensity (I_R) of the

(110) rutile peak tends to zero and a pure anatase phase is obtained. However, one may notice that some residual other small rutile peaks can still be seen beyond 0.2 at.% of Pt (Fig. 3b), so that the observed behavior may not completely be described by the Spurs formula [25]. Nevertheless, the main rutile (110) peak has completely disappeared from the XRD pattern. This suggest that, for Pt contents beyond 0.2 at.%, some residual rutile crystallites may still form in an otherwise predominant anatase polycrystalline structure. Such an occurrence reflects the complex influence of Pt incorporation on the crystalline structure of TiO_2 .

Figure 4 shows the AFM 2D scans of $\text{TiO}_2\text{:Pt}$ films as a function of their Pt content doping for both $T_d = 25$ and $500\text{ }^\circ\text{C}$. The surface morphology of the $\text{TiO}_2\text{:Pt}$ films deposited at $T_d = 25\text{ }^\circ\text{C}$ is seen to be very smooth and featureless, regardless of their Pt content, consistently with their amorphous structure revealed by XRD (see Fig. 3a), regardless Pt content (Fig. 4a, b). On the other hand, the $\text{TiO}_2\text{:Pt}$ films deposited at $T_d = 500\text{ }^\circ\text{C}$ exhibit a rougher surface than at $T_d = 25\text{ }^\circ\text{C}$ where some regular features can be easily distinguished (Fig. 4c, d). In fact, the film roughness (RMS) of the $\text{TiO}_2\text{:Pt}$ films was derived and plotted against their Pt content in Fig. 5. It is seen that the roughness of the $\text{TiO}_2\text{:Pt}$ films reaches a minimum at the 0.2 at.% of Pt for both $T_d = 25$ and $500\text{ }^\circ\text{C}$ (see Fig. 5). One may also notice (Fig. 4c, d) that the roughness of the $\text{TiO}_2\text{:Pt}$ films deposited at 25 and $500\text{ }^\circ\text{C}$ relatively decreases as the Pt content increases; this behavior is valid below a Pt concentration of 0.2 at.%, regardless the deposition temperature (Fig. 5). Nevertheless, RMS decreases monotonically at high deposition temperature ($T_d = 500\text{ }^\circ\text{C}$). For Pt contents ranging between 0 and 0.2 at.% and for a deposition temperature of $500\text{ }^\circ\text{C}$, the important decrease of the RMS may be explained by the fact that the surface mobility of the

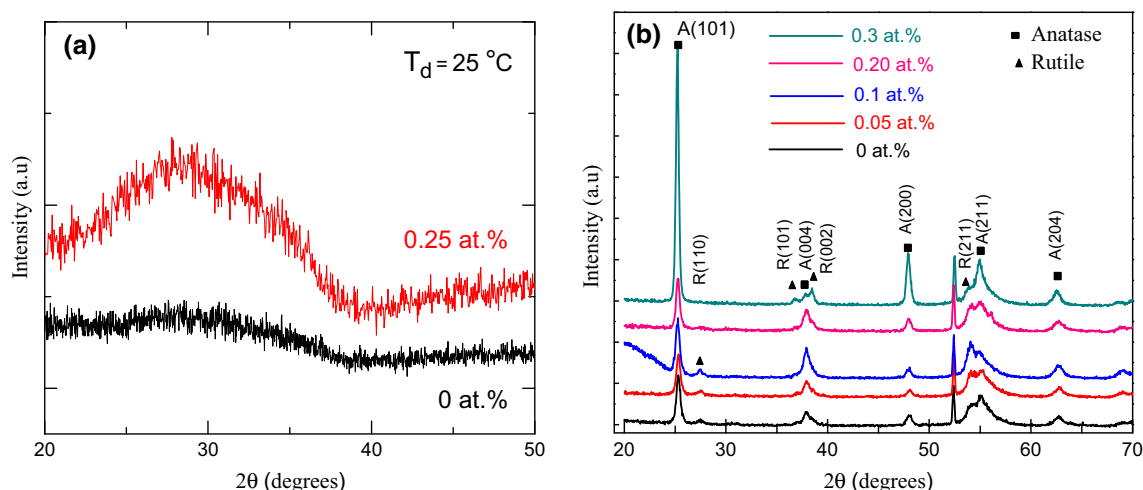
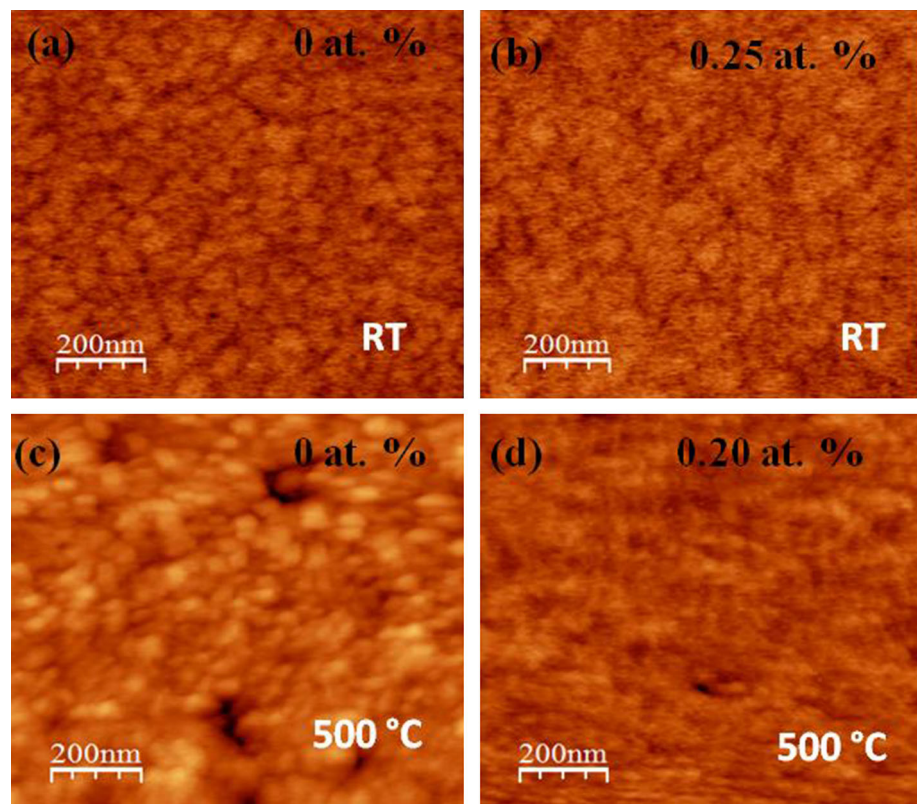


Fig. 3 a Typical XRD patterns of PLD-based $\text{TiO}_2\text{:Pt}$ films deposited at $T_d = 25\text{ }^\circ\text{C}$ and **b** at $T_d = 500\text{ }^\circ\text{C}$ for various Pt concentrations

Table 1 Effect of Pt content on the structural parameters of the PLD-TiO₂:Pt as extracted from the XRD patterns of Fig. 3b and by using Scherer, Bragg and Spurs formulas

Pt concentration (at.%)	2θ	hkl	FWHM (°)	D (nm)	Lattice parameters (Å)	W _A (%)
0	25.3	(101)A	0.45	18	a = 3.786	87
	27.5	(110)R	0.14	50	b = 9.760 c/a = 2.57	
0.05	25.3	(101)A	0.46	17	a = 3.784	85
	27.5	(110)R	0.14		c = 9.49 c/a = 2.5	
0.1	25.26	(101)A	0.46	17	a = 3.794	88
	27.5	(110)R	0.3	27	c = 10 c/a = 2.635	
0.2	25.3	(101)A	0.41	20	a = 3.79	100
					c = 9.71 c/a = 2.56	
0.3	25.22	(101)A	0.32	25	a = 3.796	100

Fig. 4 Typical AFM 2D-scans of PLD-TiO₂:Pt films at various Pt doping, deposited at T_d = 25 °C (RT) (a, b) and at T_d = 500 °C (c, d)



adatoms is higher in this temperature range, resulting in an enhanced surface diffusion length leading to island separation and lateral size growth [26].

For the observed decrease of roughness of the TiO₂:Pt (for T_d = 500 °C), one may also invoke some structural changes and/or film densification as their Pt content is increased. In fact, the SEM observations (Fig. 6) revealed that under the same PLD conditions, the film thickness halved as Pt content increases in the 0–0.2 at.% range,

regardless of T_d. Such a film densification is in accordance with the rutile-to-anatase transformation revealed by the above discussed XRD results.

To determine the optical constants and the band-gap energy from ellipsometry measurements the structure of the films was assimilated to three layers (air/TiO₂/SiO₂) over a silicon substrate. The optical constants are determined using the Forouhi–Bloomer model [27]. For T_d = 25 °C, the refractive index of the TiO₂:Pt films is found to decrease as

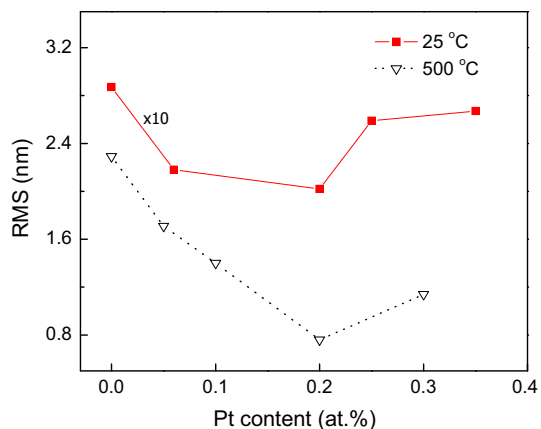


Fig. 5 Effect of the deposition temperature and Pt content on film roughness

their Pt content decreases from 0 to 0.2 at.% (Fig. 7). The TiO_2 :Pt films deposited at 25 °C exhibit a refractive index minimum value (2.25) at a Pt concentration of 0.2 at.% (Fig. 7a), which may further explain the diminution of the RMS (Fig. 5) [27]. The TiO_2 :Pt films deposited at $T_d = 500$ °C (Fig. 7b) show a continuous decrease of their refractive index with increasing Pt content down to a value of 2.45 at the Pt content of 0.3 at.%. Referring to XRD, this result can be attributed to the fact that almost all Pt-doped

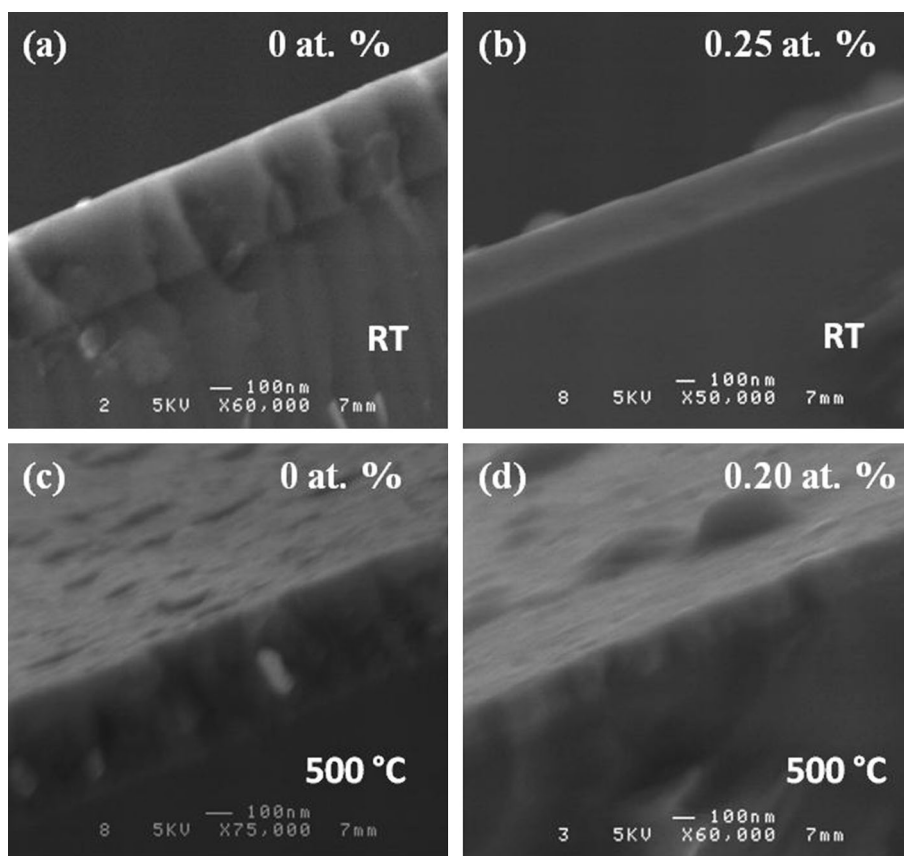
TiO_2 films transform in the crystalline anatase phase as Pt content increases, while recalling that the anatase phase is less dense than the rutile one [28].

Figure 8 shows the variation of the band gap energy (E_g) of the TiO_2 :Pt films as a function of their Pt content. The films deposited at 25 °C show a relative increase of E_g with Pt content, while those deposited at $T_d = 500$ °C exhibited in contrast an important decrease of their E_g (from 2.9 eV for pure TiO_2 to 2.45 eV for 0.25 at.% Pt doped TiO_2). This important reduction of E_g is attributed to the creation of additional levels in the bandgap of TiO_2 by incorporated Pt atoms leading to its significant narrowing [29].

Given the observed narrowing of the bandgap of the TiO_2 :Pt films deposited at $T_d = 500$ °C, their photocatalytic activities were investigated as a function of their Pt content, by testing their capacity to photo-degrade methylene blue under UV germicidal lamp (Osram, 16 W, $\lambda = 256$ nm) during 30 min. The remaining methylene blue concentration (post-degradation) was measured at 654 nm using a UV–Vis spectrophotometer.

After 30 min of illumination under UV light the dye solution shows a rapid discoloration. Figure 9 shows UV–Vis spectra of methylene blue before and after photocatalytic degradation tests of the PLD- TiO_2 :Pt films as a function of their Pt content. One may notice that TiO_2 :Pt

Fig. 6 Cross-section SEM micrographs of TiO_2 films versus deposited temperature for various Pt concentration



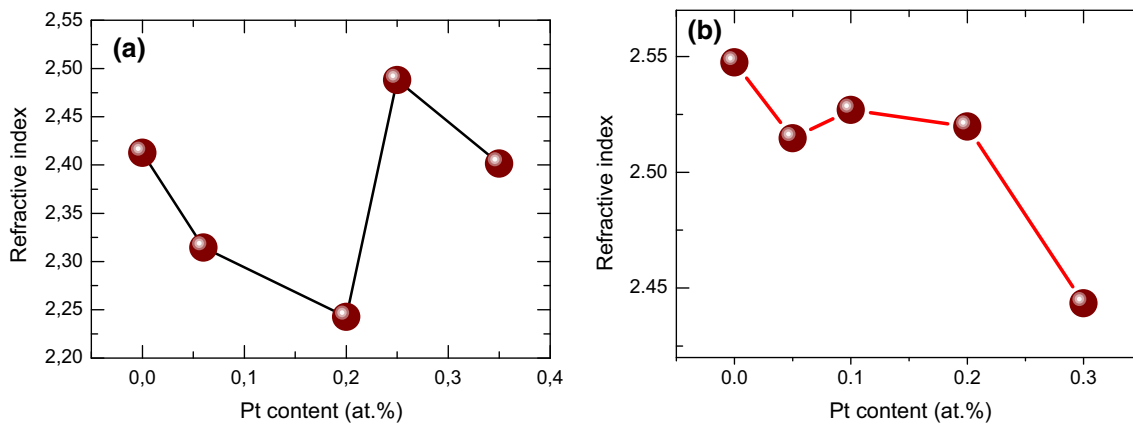


Fig. 7 Effect of Pt concentration on the refractive index values of the TiO₂:Pt films (measured at 630 nm) as a function of Pt concentration: **a** deposited at 25 °C and **b** deposited at 500 °C

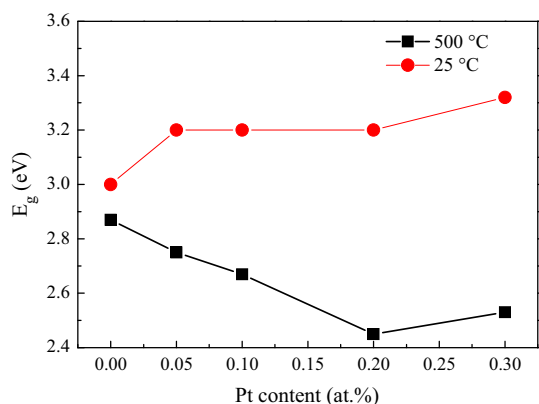


Fig. 8 Effect of Pt concentration on the band gap energy of TiO₂ films deposited at 25 and 500 °C

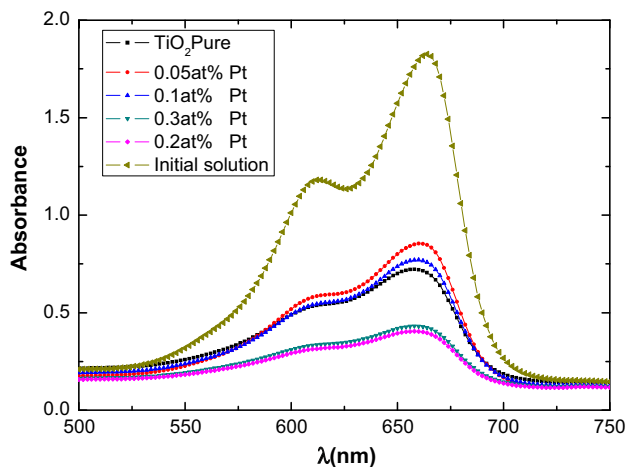


Fig. 9 UV-Vis absorbance spectra of methylene blue before and after 30 min photocatalytic degradation by the PLD-TiO₂:Pt films as a function of their Pt content

films doped with 0.2 and 0.3 at.% of Pt exhibit the highest photocatalytic activity. This high performance can be explained by two facts: (1) the lowest proportion of rutile

phase in these films, as the indirect bandgap of anatase known to be more appropriate for photocatalytic degradation [29], and most importantly (2) the narrowed bandgap of the PLD-TiO₂:Pt films allows for the photoconversion of not only UV photons (around the 3.2 eV bandgap of the anatase) but also part of the visible photons of which energies are comprised between 2.45 and 3.2 eV.

4 Conclusion

The PLD method was successfully used to deposit nanostructured, in situ Pt-doped TiO₂:Pt thin films. The in situ Pt doping approach leads to a uniform doping. Positioning 3 Pt wires on the TiO₂ target was found to lead to the incorporation of the highest Pt concentration. The Pt inclusions were found to be under both metallic and oxidized states. The crystalline structure was shown to be sensitive to the Pt content for the PLD-TiO₂:Pt films deposited at 500 °C. The surface roughness of the PLD-TiO₂:Pt films was found to be more dependent on the deposition temperature than on the incorporated Pt content. The Pt incorporation into the TiO₂:Pt films, deposited at T_d = 500 °C, was shown to be effective in narrowing their band gap energy (from ~3.0 to ~2.5 when the Pt content in increased from 0 to 0.3 at.%). This bandgap narrowing has been exploited to enhance the photocatalytic activity of the TiO₂ films. Indeed, the TiO₂:Pt films (with 0.2 at.% of Pt) were identified to be the optimum photocatalytic material leading to the highest photodegradation of methylene blue.

References

1. A. Hajjaji, K. Trabelsi, A. Atyaoui, M. Gaidi, L. Bousselmi, B. Bessais, M.A. El Khakani, *Nanoscale Res. Lett.* **9**, 543 (2014)

2. M.J. Uddin, F. Cesano, F. Bonino, S. Bordiga, G. Spoto, D. Scarano, A. Zecchina, J. Photochem. Photobiol. A **189**, 286–294 (2007)
3. R.A. Antunes, M.C.L. de Oliveira, M.F. Pillis, Int. J. Electrochem. Sci. **8**, 1487–1500 (2013)
4. M. Hosseinpour-Mashkani, M. Maddahfar, A. Sobhani-Nasab, J. Electron. Mater. **45**, 3612 (2016)
5. M. Hosseinpour-Mashkani, M. Maddahfar, A. Sobhani-Nasab, J. Mater. Sci. Mater. Electron. **27**, 474–480 (2016)
6. C.C. Evans, O. Reshef, J. Bradley, F. Parsy, J. Choy, P. Deotare, E. Martí-Panameño, M. Loncar, E. Mazur, in *TiO₂ for Nonlinear Optical Devices*, ed. by B. Di Bartolo, J. Collins. NATO Science for Peace and Security Series B: Physics and Biophysics (Springer, Netherlands, 2012), p. 405
7. A.J. Frank, N. Kopidakis, J. van de Lagemaat, Coord. Chem. Rev. **248**, 1165–1179 (2004)
8. O. Alev, E. Şennik, N. Kılınc, Z.Z. Öztürk, Proc. Eng. **120**, 1162–1165 (2015)
9. S. Li, P. Zhang, X. Song, L. Gao, ACS Appl. Mater. Interfaces **7**, 18560–18565 (2015)
10. D.A.H. Hanaor, C.C. Sorrell, J. Mater. Sci. **46**, 855–874 (2011)
11. N. Deegan, R. Dagherir, P. Drogui, M.A. El Khakani, Bandgap tailoring of in situ nitrogen-doped TiO₂ sputtered films intended for electrophotocatalytic applications under solar light. J. Appl. Phys. **116**, 153510 (2014)
12. Y. Hu, X. Song, S. Jiang, C. Wei, Chem. Eng. J. **274**, 102–112 (2015)
13. F.L. Lam, X. Hu, T.M. Lee, K.Y. Chan, Sep. Purif. Technol. **67**, 233–237 (2009)
14. T. Miyasaka, Y. Kijitori, J. Electrochem. Soc. **151**, A1767–A1773 (2004)
15. N. Janene, A. Hajjaji, M. Ben Rabha, M.A. El Khakani, B. Bessais, M. Gaidi, Phys. Status Solidi (c) **9**, 2141–2144 (2012)
16. E. Gyorgy, G. Socol, E. Axente, I.N. Mihailescu, C. Ducu, S. Ciuca, Appl. Surf. Sci. **247**, 429–433 (2005)
17. T. Yoshida, Y. Fukami, M. Okoshi, N. Inoue, Jpn. J. Appl. Phys. Part 1 Regul. Pap. Brief Commun. Rev. Pap. **44**, 3059–3062 (2005)
18. D. Gonbeau, C. Guimon, G. Pfisterguillouzo, A. Levasseur, G. Meunier, R. Dormoy, Surf. Sci. **254**, 81–89 (1991)
19. C.M. Chan, S. Trigwell, T. Duerig, Surf. Interface Anal. **15**, 349–354 (1990)
20. S. Lars, T. Andersson, Catal. Lett. **7**, 351–358 (1990)
21. Z. Zheng, X. Wang, J. Liu, J. Xiao, Z. Hu, Appl. Surf. Sci. **309**, 144–152 (2014)
22. M.A. El Khakani, R. Dolbec, A.M. Serventi, M.C. Horrillo, M. Trudeau, R.G. Saint-Jacques, D.G. Rickerby, I. Sayago, Sens. Actuators B Chem. **77**, 383–388 (2001)
23. S.F. Wang, Y.F. Hsu, R.L. Lee, Y.S. Lee, Appl. Surf. Sci. **229**, 140 (2004)
24. A. Guinier, *Théorie et technique de la radiocristallographique* (Dunod, Paris, 1964)
25. R.A. Spurr, H. Myers, Anal. Chem. **29**, 760–761 (1957)
26. M. Reason, N.G. Rudawski, H.A. McKay, X. Weng, W. Ye, R.S. Goldman, J. Appl. Phys. **101**, 083520 (2007)
27. J.P. Jalava, V.M. Taavitsainen, R.J. Lamminmäki, M. Lindholm, S. Auvinen, M. Alatalo, E. Vartiainen, H. Haario, J. Quant. Spectrosc. Radiat. Transf. **167**, 105–118 (2015)
28. D. Mergel, D. Buschendorf, S. Eggert, R. Grammes, B. Samset, Thin Solid Films **371**, 218–224 (2000)
29. T. Fuyuki, H. Matsunami, Jpn. J. Appl. Phys. Part 1(25), 1288 (1986)